Korean Journal of Geomatics
Vol. 3, No. 1 / June 2003
pp. 33~41

Classification of Water Areas from Satellite Imagery Using Artificial Neural Networks

Hong-Gyoo SOHN*, Yeong-Sun SONG and Won-Jo JUNG*****

Abstract

Every year, several typhoons hit the Korean peninsula and cause severe damage. For the prevention and accurate estimation of these damages, real time or almost real time flood information is essential. Because of weather conditions, images taken by optic sensors or LIDAR are sometimes not appropriate for an accurate estimation of water areas during typhoon. In this case SAR (Synthetic Aperture Radar) images which are independent of weather condition can be useful for the estimation of flood areas.

To get detailed information about floods from satellite imagery, accurate classification of water areas is the most important step. A commonly- and widely-used classification methods is the ML(Maximum Likelihood) method which assumes that the distribution of brightness values of the images follows a Gaussian distribution. The distribution of brightness values of the SAR image, however, usually does not follow a Gaussian distribution. For this reason, in this study the ANN (Artificial Neural Networks) method independent of the statistical characteristics of images is applied to the SAR imagery. RADARSAT SAR images are primarily used for extraction of water areas, and DEM (Digital Elevation Model) is used as supplementary data to evaluate the ground undulation effect. Water areas are also extracted from KOMPSAT image achieved by optic sensors for comparison purpose.

Both ANN and ML methods are applied to flat and mountainous areas to extract water areas. The estimated areas from satellite imagery are compared with those of manually extracted results. As a result, the ANN classifier performs better than the ML method when only the SAR image was used as input data, except for mountainous areas. When DEM was used as supplementary data for classification of SAR images, there was a 5.64% accuracy improvement for mountainous area, and a similar result of 0.24% accuracy improvement for flat areas using artificial neural networks.

Keywords : Water area, Artificial neural network, Maximum likelihood, RADARSAT, KOMPSAT

1. Introduction

Every year, several typhoons hit the Korean peninsula and cause severe damage. For example, in August 2002, typhoon Rusa hit the Korea peninsula and the estimated damages reached about 226.5 billion won(≒ 1.9 billion dollar). For the prevention and accurate estimation of annually repeated damages from typhoons, real time or almost real time flood information is essential. Also, a large synoptic view of ground truth information is more useful than local and limited area information. For this reason, a remote sensing approach has been utilized since the launch of the LANDSAT satellite.

Flood information, however, is difficult to obtain by using optic sensors during a flood due to its dependency on the existence of light or the sun as a source of energy. Active sensors with their own source of energy have advantages over passive sensors for this kind of application. Recently, several satellites with active sensors on board were launched; ERS-1 and 2 in Europe, JERS-1 in Japan, and RADARSAT-1 in Canada. Even if weather conditions are bad or there is no light source, these satellites can produce images of the ground.

Despite these advantages over passive sensors for

*Assistant Professor, School of Civil and Environment Eng., Yonsei University (E-mail : sohn1@yonsei.ac.kr)
**Ph. D. Student, School of Civil and Environment Eng., Yonsei University (E-mail : point196@yonsei.ac.kr)
***Researcher, Sokkok Institute of Observational Science & Technology (E-mail : wonjo@sog.or.kr)

The manuscript for this paper was received on May 12, 2003 / accepted on June 30, 2003.

flood applications, SAR images contain speckle noise and shadow effect caused by side looking geometry. The presence of speckle in an image reduces the detectability of ground targets, obscures the spatial patterns of surface features, and decreases the accuracy of automated image classification (Sheng and Xia, 1996). It is necessary to enhance the image by speckle filtering before data can be used in classification. Since SAR processing does not include topographic information, radiometric corrections are omitted during the processing step, and these steps need to be considered on a postprocessing basis (Stebler et al., 1996). Therefore it is necessary to make a radiometric correction for SAR data to proceed to further processing.

Classification of water areas is one of the essential processes in flood monitoring. ML (Maximum Likelihood) method, one of the most frequently used methods in a classification, assumes that brightness values (or digital number) of the imagery follow a Gaussian distribution. For imagery from most optic sensors, this assumption is appropriate and results obtained from optic sensors have shown reasonable outcomes. Generally, it is known that the distribution of amplitude images of SAR does not follow the Gaussian distribution. For this reason, applying the ML method to SAR imagery may cause classification errors if the imagery does not follow the statistical assumption made to use the method (Decatur, 1989). On the other hand, the ANN (Artificial Neural Networks) method is independent of statistics of brightness values of imagery, so neural networks can be readily applied to the classification of SAR imagery. Generally, an ANN is capable of storing a complex functional relationship between its input (backscattered energy) and its outputs (land cover), and of approximating any function with a finite number of discontinuities (Ghedira et al., 2000). Several research efforts related this study have shown that an ANN can be used as an accurate tool in radar image classification (Park et al., 1999; Ghedira et al., 2000; Manian et al., 2000).

In Korea, several researches related with the land-use classification using ANN have been done (Jeon et al., 2000; Kang et al., 2000; Yang et al., 2000, Lim et al., 2002). ANN showed better classification result when more than one image is used (Choi et al., 2001) and detects boundary of water area more precisely than statistical classification method (Yang et al., 2002).

The main objectives of this research are three-fold; (1) accurate extraction of water areas from SAR images using an ANN, (2) comparison of classification accuracy between the ANN method and the ML method, and (3) improving the classification accuracy of water areas by adding a digital elevation model as a supplementary data set.

2. Preprocessing of Input Data

Pre-processing steps mainly included are the geometric and radiometric correction of satellite images before classification. In this study, RADARSAT SAR and KOMPSAT images are classified using both ANN and ML methods. Figure 1 depicts the schematic diagram of the entire data processing procedure for classification, and the dotted area represents the preprocessing steps peformed before actual classification of data sets.

2.1 Data Set and Study Area

In this study, study areas are separated into flat and mountainous areas (see Figure 2) to find out the

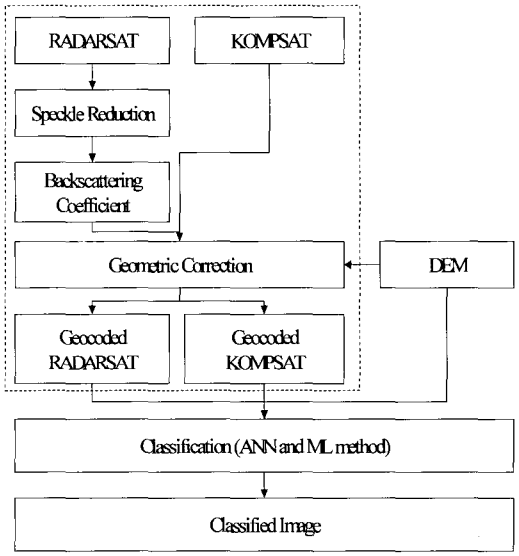

Fig. 1. Data processing procedure.

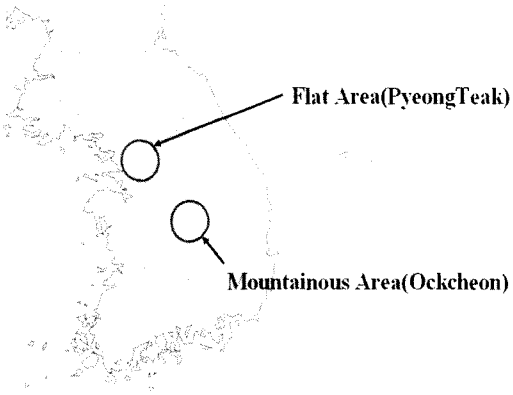

Fig. 2. Study Area.

usefulness of an ANN over the ML regardless of ground undulation. Standard deviation of DEM is 10.970m for flat areas and 77.323m for mountainous areas. For each study area, three major data sources (RADARSAT SAR image, KOMPSAT image, and DEM) were utilized. Brief scene description of RADARSAT SAR data and

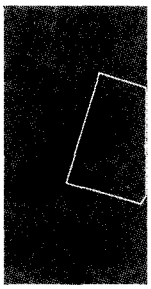

(a) KOMPSAT image

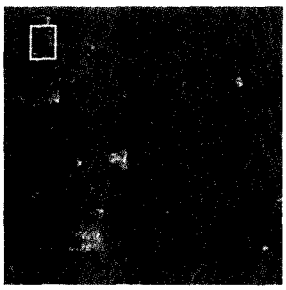

(b) RADARSAT SAR image

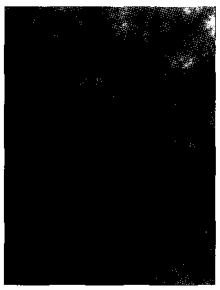

(c) DEM of Pyeonteak Area

Fig. 3. Data set of flat area.

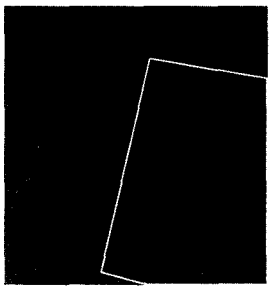

(a) KOMPSAT image

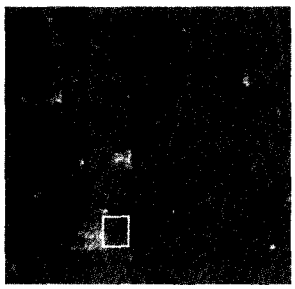

(b) RADARSAT SAR image

(c) DEM of Ockcheon Area

Fig. 4. Data set of mountainous area.

Table 1. Scene description of RADARSAT

Scene start time	August 12, 1998 09:34:28.589
Scene stop time	August 12, 1998 09:34:45.887
Orbit	14461 Ascending
Beam mode	SAR Standard 6
Product type	Path Image (SGF)
Format	RADARSAT CEOS
Pixel Spacing	12.500m
Scene Center	36°41'N, 127°33'E

Table 2. Scene descriptions of KOMPSAT

	Ockcheon Area	Pyeongteak Area
Scene center time	March 3, 2000, 01:52:00.568	May 8, 2000, 01:43:25.041
Orbit	1032	2025
Look angle	3.8641°	21.768°
Incidence angle	4.2799°	24.248°
Orientation angle	10.008°	10.081°
Pixel spacing	6.6m	6.6m
Scene center	36.263°, 127.5°	36.819°, 127.06°

that of KOMPSAT is summarized in Table 1 and 2, respectively. DEM is generated from a 1:5,000 scale digital map for the Ockcheon area and a 1:25,000 scale map for Pyeongteak area. DEMs created from each data set are represented in Figure 3(c) and Figure 4(c), respectively.

2.2 Speckle Noise Reduction

Speckle appears on all SAR products including single-polarimetric, multipolarimetric, and interferometric image data (Dong et al., 2000). The presence of speckle in an image reduces the detectability of ground targets, obscures the spatial patterns of surface features, and decreases the accuracy of automated image classification (Sheng and Xia, 1996). Thus, it is necessary to enhance the image by speckle filtering before data can be used in applications. Typical noise smoothing methods such as moving average and median filter are not well suited for preserving edges. Zaman and others (1993) compared several filters using the category of radiometric value preservation in single look and multilook polarimetric SAR images and concluded that the Lee filter was the best. In this research, the improved Lee-sigma filter was applied to RADARSAT SAR images for speckle noise reduction.

2.3 Calculation of Backscattering Coeffieicnt

To perform classification of SAR data, the DN values have been transformed into backscattering coefficients. The procedure from DN value to σ^0 (a radar backscattering coefficient) is done as follows(Logan T, 1999: RSI, 2000):

$$\beta_j^0 = 10 \times \log_{10}[(DN_j^2 + A_3)/A_{2j}] \quad (1)$$

where, A_{2j} is the scaling gain value of the jth pixel in the slant range direction determined by interpolating 512 LUT values given at the header, A_3 the scaling offset, and DN_j the digital value of the jth pixel. The relationship between radar brightness (β_j^0) and the radar backscattering coefficient is given by

$$\sigma_j^0 = \beta_j^0 + 10 \log_{10}(\sin I_j) \quad (2)$$

where, I_j is the incidence angle at the jth range pixel. This formula assumes that the earth is smooth ellipsoid at sea level. Calculation of I_j is done by using the formula given by

$$I_j = \cos^{-1}\left[\frac{(h^2 - (r_j)^2 + 2 \cdot R \cdot h)}{2 \cdot r_j \cdot R}\right] \quad (3)$$

where, R is the earth radius at the image center position, h is the orbit altitude, and r_j is the slant range of the jth pixel.

2.4 Geocoding of Satellite Image

After backscattering coefficients are calculated, to use DEM as a supplementary input data of the artificial neural network, geocoding of satellite images was performed. Exact estimation of the satellite's position is one of the crucial procedures for the ortho-rectification. The RADARSAT SAR image was orthorectified using 20m resolution DEM and twenty GCPs by range, and the Doppler centroid Equation method (Schreier, 1993; Sohn et al., 2002). For the geocoding of KOMPSAT imagery, the generic pushbroom module of ERDAS IMAGINE 8.0 was used. Twenty six ground control points (GCPs) were used for the Pyeongteak area and twenty five GCPs were used for the Ockcheon area. The results of ortho-rectified satellite imagery are shown in Figure 5.

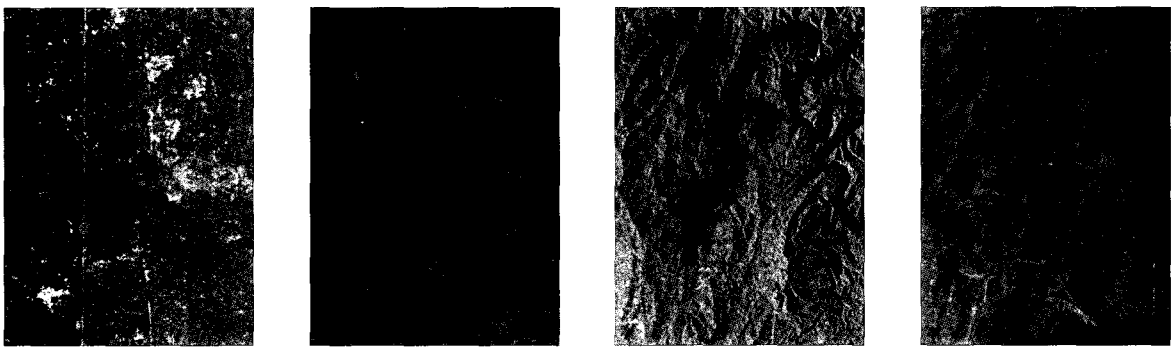

(a) RADARSAT (b) KOMPSAT (c) RADARSAT (d) KOMPSAT

Fig. 5. Geocoded Images; (a) and (b) are flat area, (c) and (d) are mountainous area.

3. Classification Using Artificial Neural Networks Algorithms

3.1 Artificial Neural Networks Algorithms

ANNs have been widely used in pattern recognition, and in many image classification applications (Lee et al., 1999). Recently, neural networks have been applied to a number of image classification problems and have shown considerable success in matching or exceeding the performance of conventional algorithms (Herman and Khazenie, 1992). This success stems from the ability of artificial neural networks to overcome several of the limitations of conventional algorithms. The most severe limitation is that a conventional classification algorithm presumes that input data has a particular form. For example, the ML method assumes that the probability density function of the brightness values (digital numbers) follows a Gaussian distribution. If the data the indeed follows a presumed particular form, and an appropriate model which can classify the presumed particular form exists, then conventional methods may work well.

However, the chosen particular forms may be suboptimal and the classification result may be poor. The ANN method does not presume the input data as being of a particular form. In problems requiring utilization of data from several sources of unequal reliability, neural networks are capable of automatically determining the relative reliabilities of the sources during training, and adjusting the network to achieve the appropriate change in the internal classification algorithm represented by the network (Benediktsson et al., 1990).

Following is a brief description of ANN algorithms used in this study. A neuron, the information processing unit, is the basic element of an ANN. The following equation is the mathematical model of the neuron used in this study (See Equation 4).

$$y_k = \varphi(\nu_k) = \varphi\left(\sum_{j=1}^{m} w_{kj}x_j + b_k\right) \quad (4)$$

When input data, $x_1, x_2, \cdots x_m$, is the entered neuron, weights ($w_{k1}, w_{k2}, \cdots, w_{km}$) are multiplied to input data, and bias b_k is applied through Equation 4. The linear sum of the weighted input data is called the induced local field ν_k. $\varphi(\nu)$ is the activation function that is a S-shaped non-linear sigmoid function, and its output signal varies from -1 to 1 (See Equation 5).

$$\varphi(\nu) = \frac{1}{1+\exp(-a\nu)} \quad (5)$$

A perceptron consists of neurons, and the most simple form of the perceptron is a single neuron. A neuron can be positioned on the decision surface in the form of a hyperplane between the two classes. In the literal sense of the word, a multilayer perceptron consists of more than one layer of perceptrons. In this study, a fully connected feed forward multilayer perceptron was used for the classification.

To obtain the desired output from an ANN, the network should be trained. In this study, a BP (Back Propagation) algorithm was used. BP algorithm basically consists of a forward and a backward pass. During the forward pass, input data is entered to the networks and its effects propagate through the network, layer by layer. Finally, the actual responses of the networks are produced. During the backward pass, the error between actual response and desired response propagates by error correction rules.

Figure 6 shows the structure of the ANN used in this study. The ANN consisted of two hidden layers and had two output nodes. To avoid localization during the BP algorithm, backscattering coefficients and DEM values were normalized.

A two dimensional input consisting of a backs-cattering coefficient and elevation from DEM was

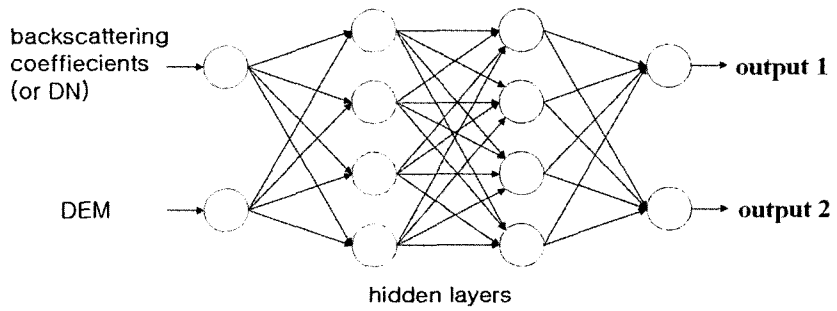

Fig. 6. Structure of ANN(Artificial Neural Networks) used in this study.

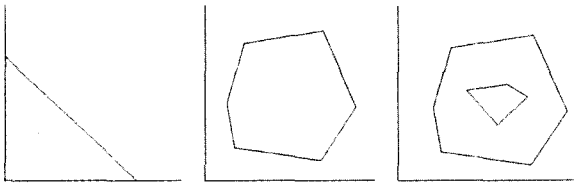

(a) no hidden layer was used (b) one hidden layer was used (c) more than two hidden layers were used

Fig. 7. Illustration of some of the possible decision boundaries.

used for RADARSAT SAR image classification. For KOMPSAT image classification, a DN value was used instead of a backscattering coefficient. Some of the possible decision boundaries are shown in Figure 7 according to the number of hidden layers. Artificial neural networks having two hidden layers of weights can generate arbitrary decision regions as shown in Figure 7(c).

3.2 Classification Results

For one study area, six combinations of data sets (see Table 3) were applied to the classifiers. A total of twelve combinations of data sets for flat and mountainous areas were chosen. Statistical values of input data sets and training data sets are listed in Table 4 and 5. ANN classifier networks had two input nodes. One was for backscattering coefficients of the RADARSAT SAR image (DN for KOMPSAT image), and the other was for DEM. Input values went through two hidden layers of neurons. Then finally there were two output nodes (See Figure 6).

In case 6, RADARSAT SAR images were classified by the ML method. Then a boolean operation was applied to the classified image with DEM. Classified image are shown at Figure 8 and 9. For the accuracy analysis, each image was classified manually. Manually

Table 3. Input data combination

Case	Combinations of data sets	Classifier
1	RADARSAT SAR image only	ANN
2	KOMPSAT image only	ANN
3	RADARSAT SAR and DEM	ANN
4	RADARSAT SAR image only	ML
5	KOMPSAT image only	ML
6	RADARSAT SAR and DEM	ML & Boolean

Table 4. Statistical values of input data sets

	Min.	Max.	Mean	Standard Deviation
KOMPSAT (Pyeongteak)	0	196	75.344	33.902
KOMPSAT (Ockcheon)	0	91	37.514	17.953
RADARSAT	-25.03	8.183	-8.216	3.976
DEM (Pyeongteak)	-1.1339	127.04	18.496	10.970
DEM (Ockcheon)	0	583.83	139.338	77.323

Table 5. Statistical values of training sets

	Water areas (4800 pixels)				Non-water areas (4800 pixels)			
	Min.	Max.	Mean	Standard Deviation	Min.	Max.	Mean	Standard Deviation
KOMPSAT (Pyeongteak)	50	95	55.91	8.717	60	135	84.29	23.27
KOMPSAT (Ockcheon)	33	37	34.96	0.316	39	88	56.52	38.19
RADARSAT (Pyeongteak)	-25.03	-3.13	-20.62	16.75	-23.20	60.54	21.01	25.73
RADARSAT (Ockcheon)	-25	-8	-19.93	12.566	-25.03	5.199	-10.41	23.98
DEM (Pyeongteak)	9.99	10.0	10.0	0.0000001	0.99	60.54	21.01	17.43
DEM (Ockcheon)	59.98	73.83	67.34	5.597	63.67	410.96	202.63	37.21

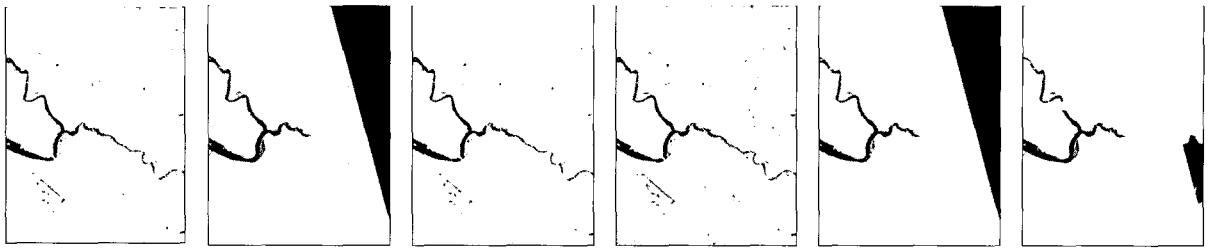

(a) Case 1 (b) Case 2 (c) Case 3 (d) Case 4 (e) Case 5 (f) Case 6

Fig. 8. Results for flat areas.

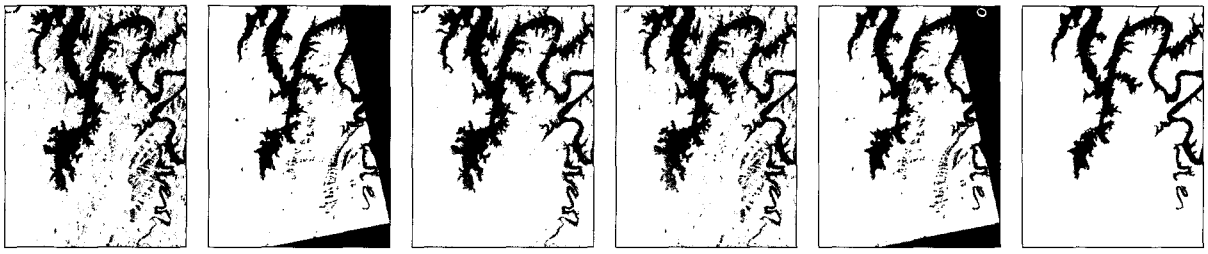

(a) Case 1 (b) Case 2 (c) Case 3 (d) Case 4 (e) Case 5 (f) Case 6

Fig. 9. Results for mountainous areas.

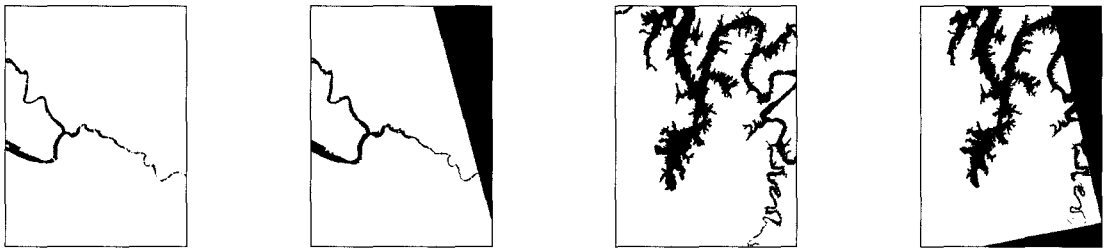

(a) RADARSAT (b) KOMPSAT (d) RADARSAT (d) KOMPSAT

Fig. 10. Manually classified images: (a), (b) for flat areas, and (c), (d) for mountainous areas.

classified images were used for the reference data, and the results of manual classification are shown in Figure 10.

4. Analysis

For the accuracy analysis, an error matrix was calculated, and Table 6 shows classification accuracies for each case. The Artificial Neural Network classifier performed better than maximum likelihood when single satellite imagery was used, except for the SAR image of mountainous areas. For mountainous areas, curve fitting of the backscattering coefficients and Chi-square test was performed. Level of significance was 5 percent. The result of Chi-square test was that the distribution of backscattering coefficients does not follow the Gaussian distribution. Therefore, the reason why maximum likelihood method performed better than artificial neural networks in mountainous areas was not a distribution problem but due to other factors.

When we used the DEM as supplementary data of classifiers, maximum likelihood seems to perform statistically better than artificial neural networks. The problem for this case was that during the Boolean operation, noise of non-water areas was almost removed. When considering the object of this research, classification accuracy of water areas is more important than that of non-water areas. Even though maximum likelihood method outperforms the overall accuracy, there was too much loss of water area information. When we compared the water area classification accuracy instead of overall accuracy in backscattering coefficient and DEM, artificial neural networks perform better than maximum likelihood methods, 3.07% for a flat area and 16.39% for a mountainous area. The dotted circle areas in Figure 11 show the information loss of

Table 6. Accuracy of classification (unit : %)

		KOMPSAT			Backscattering Coeffieicnt			Backscattering Coefficient and DEM		
		overall accuracy	classification accuracy		overall accuracy	classification accuracy		overall accuracy	classification accuracy	
			water	non -water		water	non -water		water	non -water
Flat Area	ANN	98.55	82.15	99.08	97.82	77.77	98.27	98.06	78.53	98.50
	ML	98.52	75.80	99.23	96.64	80.55	97.00	97.98	75.46	98.48
	Superior Classifier	ANN	ANN	ML	ANN	ML	ANN	ANN	ANN	ANN
	Accuracy difference	0.03	6.35	0.15	1.18	2.78	1.27	0.08	3.07	0.02
Mountainous Area	ANN	94.43	89.45	95.39	87.67	97.15	85.52	93.31	93.29	89.32
	ML	93.65	87.19	94.89	90.41	94.95	89.38	93.43	76.90	97.18
	Superior Classifier	ANN	ANN	ANN	ML	ANN	ML	ML	ANN	ML
	Accuracy difference	0.78	2.26	0.5	2.74	2.2	3.86	0.12	16.39	7.86

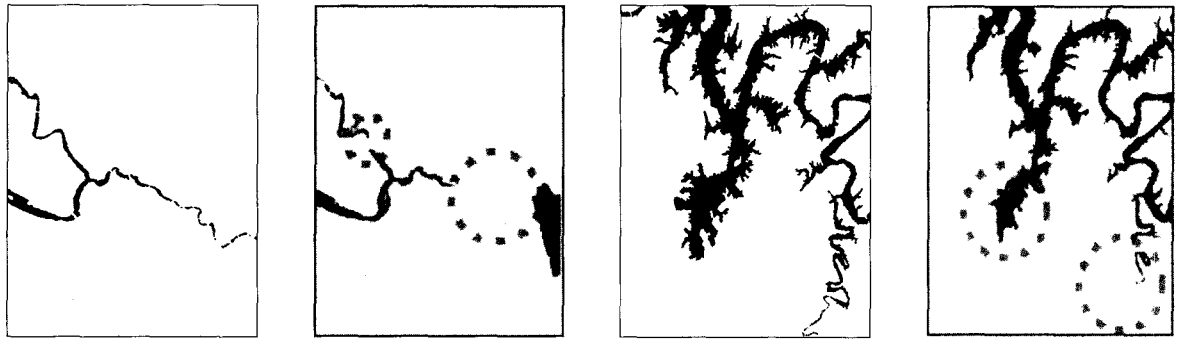

(a) (b) (c) (d)

Fig. 11. Information loss of water areas; (a) and (c) are manually classified results, (b) and (d) are results of the maximum likelihood method with Boolean operation. (a) and (b) are flat areas and, (c) and (d) are mountainous areas.

the water areas when ML and Boolean operations were applied to the backscattering coefficients.

5. Conclusion

After applying the artificial neural networks classification method to RADARSAT SAR and KOMPSAT imagery, the following conclusions have been reached.

1. Artificial neural networks perform better than the maximum likelihood method when single SAR imagery was used, except for the mountainous areas.

2. When DEM was used for supplementary data for classification, overall accuracy of ML and Boolean methods were higher than the overall accuracy of the ANN. But, ML and Boolean methods lose too much information of water areas. When we compare the water area classification accuracy instead of overall accuracy, ANN performed better than ML method 3.07% for a flat area and 16.39% for a mountainous area.

3. It was possible to accurately estimate water areas from a SAR image using an artificial neural network classifier. It can be considered that a neural network classifier with DEM data can be used for upcoming flood monitoring.

Acknowledgements

This works was supported by grant No. 2000-1-0093 from Research Program of Yonsei University.

References

1. 강호윤, 강인준, 최현, 이승찬, 2000, 신경망을 이용한 인공위성 영상분류 정확도에 관한 평가, 대한토목학회 학술발표

회 논문집(IV), pp. 585-588.
2. 양인태, 김홍규, 박재국, 조성배, 2000, 신경망 이론과 퍼지 집합 이론을 이용한 위성영상의 분류 정확도에 관한 연구, 대한토목학회 학술발표회 논문집(IV), pp. 589-592.
3. 양인태, 한성만, 박재국, 2002, 원격탐사 영상의 분류정확도 향상을 위한 인공지능형 시스템의 적용, 한국측량학회지, 제20권, 제1호, pp. 21-31.
4. 임승현, 이근상, 양옥진, 조기성, 2002, 유전자 및 역전파알고리즘을 적용한 신경망연산에 의한 토지적합성분석, 대한토목학회 논문집, 제22권, 제6-D호, pp. 1317-1326.
5. 전형섭, 정승현, 박성규, 조기성, 2000, 신경망에 의한 토지피복분류의 정확도 향상에 관한 연구, 대한토목학회 학술발표회 논문집(IV), pp. 817-820.
6. 전형섭, 조기성, 토지피복분류에 있어 신경망과 최대우도분류기의 비교, 2000, 한국지형공간정보학회논문집, 제8권, 제2호, pp. 23-33
7. 최현, 강인준, 홍순헌, 2001, 신경망을 이용한 합성영상에서의 분류 정확도에 대한 평가, 대한토목학회논문집, 제21권, 1-D호, pp. 115-123.
8. Benediktsson, J. A., H. S. Philip, and O. K. Ersoy, 1990, Neural Network Approaches Versus Statistical Methods in Classification of Multisource Remote Sensing, IEEE Transaction on Geoscience and Remote Sensing, Vol. 28, No. 4, pp. 540-551.
9. Decatur, S. E., 1989, Application of Neural Networks to Terrain Classification, Proceedings of the IEEE International Joint Conference on Neural Networks, pp. 283-288.
10. Dong, Y., A. K. Milne, and B. C. Forster, 2000, A Review of SAR Speckle Filters: Texture Restoration and Preservation, Proceedings Geoscience and Remote Sensing Symposium, IEEE 2000 International, Vol. 2, pp. 633-635.
11. Ghedira, H., M. Bernier, and T.M.B.J. Ouarda, 2000, Application of Neural Networks for Wetland Classification in RADARSAT SAR Imagery, IGARSS 2000, Vol. 2, pp. 675-677.
12. Herman, P.D. and N. Khazenie, 1992, Classification of earth terrain using polarimetric synthetic aperture radar images, Journal of Geophys. Res., Vol. 94, No. B6, pp. 7049-7057.
13. Lee, C., P. Chung, J. Tsai, and C. Chang, 1999, Robust radial basis function neural networks, IEEE Transactions on SMC, Part B, Vol. 29, No. 6, pp. 674-685.
14. Logan, T., 1999, Calculation of ASF CEOS Metadata Values.
15. Manian, V., R. Hernandez, R. Vasquez, 2000, Classifier Performance for SAR Image Classification, IGARSS 2000, Vol. 1, pp. 156-158
16. Park, J. D., L. Jones, and J. Zec, 1999, Sea Ice Classification using a Neural Network Algorithm for NSCAT, IGARSS 99, Vol. 2, pp. 1040-1043.
17. RSI, 2000, RADARSAT Data Products Specifications.
18. Schreier, G., 1993, SAR geocoding : data and systems, Wichmann, pp. 103-133.
19. Sheng, Y. and Z. Xia, 1996, A Comprehensive Evaluation of Filters for Radar Speckle Suppression, IGARSS 96, Vol. 3, pp. 1559-1561.
20. Sohn, H. G., Y. S. Song, H. H. Yoo, W. J. Jung, 2002, Estimation of the Flood Area Using Multi-temporal RADARSAT SAR Imagery, Korean Journal of Geomatics, Vol. 2. No. 1, pp. 37-46
21. Stebler, O., P. Pasquali, D. Small, F. Holecz, and D. Nuesch, 1996, Analysis of ERS-SAR Tendem Time-Series Using Coherence and Backscattering Coefficient, ESA Workshop on Application of ERS SAR Interferometry
22. Zaman, M. R. and C. R. Moloney, 1993, A Comparison of Adaptive Filters for Edge-preserving Smoothing of Speckle Noise, IEEE Transaction on Geoscience and Remote Sensing, pp. 77-80.